A pair potentials study of matrix-isolated atomic zinc. II. Intersystem crossing in rare-gas clusters and matrices

W. H. Breckenridge[a] M. D. Morse, and John G. McCaffrey[b]
Department of Chemistry, University of Utah, Salt Lake City, Utah 84112

(Received 6 April 1998; accepted 19 May 1998)

The mechanism of $4p\ ^1P_1 \rightarrow 4p\ ^3P_J$ intersystem crossing (ISC) following excitation of the $4p\ ^1P_1$ level of matrix-isolated atomic zinc is investigated using a pair potentials approach. This is achieved by extending earlier ISC calculations on the $Zn\cdot RG_2$ and $Zn\cdot RG_3$ complexes to the square planar $Zn\cdot RG_4$ and square pyramidal $Zn\cdot RG_5$ species which are the building blocks of the $Zn\cdot RG_{18}$ cluster used to represent the isolation of atomic zinc in the substitutional site of a solid rare-gas host. ISC predictions in these clusters are based on whether crossing of the strongly bound $^1A_1$ states, having a $4p\ ^1P_1$ atomic asymptote, occurs with the repulsive ^3E states correlating with the $4p\ ^3P_J$ atomic level of atomic zinc. Predictions based on $^1A_1/^3E$ curve crossings for ^3E states generated with the calculated *ab initio* points for the $Zn\cdot RG\ ^3\Sigma(p_z)$ states do not agree with matrix observations. Based on similar overestimation of ISC in the Zn·RG diatomics, less repulsive $Zn\cdot RG\ ^3\Sigma(p_z)$ potential curves are used resulting in excellent agreement between theory and observations in the Zn–RG matrix systems. $^1A_1/^3E$ curve crossings do not occur in the Zn–Ar system which shows only singlet emission. Curve crossings are found for the Zn–Xe system which exhibits only triplet emission. The Zn–Kr system does not show a crossing of the body mode Q_2, which exhibits a strong singlet emission at 258 nm while the waist mode Q_3, does have a crossing, resulting in a weak singlet emission at 239 nm and a stronger triplet emission at 312 nm. The efficiency of ISC is determined from Landau–Zener estimates of the surface hopping probabilities between the $^1A_1$ and the ^3E states. Differences in the application of this theory in the gas and solid phase are highlighted, indicating that the rapid dissipation of the excited-state energy which occurs in the solid must be included to obtain agreement with observations. © *1998 American Institute of Physics.* [S0021-9606(98)00532-7]

I. INTRODUCTION

Matrix-isolated atomic zinc has been examined in detail[1] both experimentally, with luminescence spectroscopy, and theoretically, from a pair potentials approach. A key feature of the luminescence spectroscopy in the Zn–RG matrix systems (RG=rare gas) is the existence of pairs of emission bands. A summary of the luminescence spectroscopy in the Zn–RG systems is presented in Fig. 1 for annealed samples at 9 K. By exploiting the intrinsic fourfold symmetry of the cubooctahedral substitutional site, McCaffrey and Kerins[1] developed a $Zn\cdot RG_{18}$ cluster model which accounted for the pairs of emission bands observed in the Zn–RG matrix systems. Two vibronic modes were identified as being responsible for the production of the pairs of emission bands following photoexcitation of the $4p\ ^1P_1 \leftarrow 4s\ ^1S_0$ absorption band. An in-phase contraction of four rare-gas atoms on a plane towards the zinc atom, labeled the ''waist'' mode Q_3, produced the higher energy emission bands while motion of the guest zinc atom towards one of the two octahedral interstitial sites adjacent to the substitutional site occupied in the ground state, the ''body'' mode Q_2, produced the lower energy bands.

Another key feature of the luminescence in the Zn–RG matrix systems[2] shown in Fig. 1, is the different extents of $4p\ ^1P_1 \rightarrow 4p\ ^3P_J$ intersystem crossing (ISC) occurring for atomic zinc isolated in Ar, Kr, and Xe hosts after $4p\ ^1P_1$ excitation. As shown in Fig. 1, only a pair of spin singlet emission bands are observed in the Zn–Ar system[2,3] at 219 and 238 nm without any trace of spin triplet emission. For Zn–Kr, as in the Zn–Ar system, a pair of spin singlet bands are observed at 239 and 258 nm, but in this case with very different intensities. In starker contrast to the Zn–Ar system, there is also a triplet emission band at 312 nm in Zn–Kr, the intensity of which is temperature dependent.[2] Excitation into the singlet $4p\ ^1P_1 \leftarrow 4s\ ^1S_0$ absorption band of Zn–Xe produces no spin singlet emission at all, with emission occurring only as the pair of spin triplet bands at 356 and 399 nm.

The results for ISC in the Zn–RG matrix systems can be compared to the simpler situation of the gas phase, where the $Zn(4s4p\ ^1P_1)$ state interacts with only one rare-gas atom. The evidence is strong that ISC is very inefficient for both Ar and Kr atoms, while it is moderately efficient for Xe. In ''full-collision'' studies it is known that the cross section for deactivation of $Zn(4s4p\ ^1P_1)$ by Ar is extremely low[4] ($<5\times10^{-4}$ Å^2, or less than one deactivation per 10^5 collisions), while that for the deactivation of $Zn(4s4p\ ^1P_1)$ by Xe is moderate[5] (3.8 Å^2, one deactivation in 10 collisions). In the $Zn(^1P_1)+Xe$ collision work of Umemoto and

[a]E-mail: breckenridge@chemistry.utah.edu
[b]Visiting Associate Professor 1998. Permanent address: Department of Chemistry, National University of Ireland, Maynooth, Co. Kildare, Ireland.

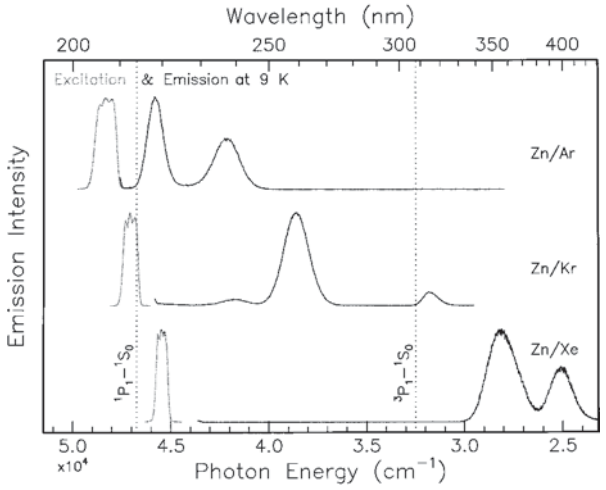

FIG. 1. Excitation and emission spectra recorded at 9 K in the annealed Zn–RG matrix systems. The excitation wavelengths used in producing the emission spectra were 207, 212, and 220 nm for Zn–Ar, Zn–Kr, and Zn–Xe, respectively. The spectral positions of the resonance singlet $4s4p\ ^1P_1-4s^2\ ^1S_0$ and triplet $4s4p\ ^3P_1-4s^2\ ^1S_0$ transitions of atomic zinc in the gas phase are shown by the dotted vertical lines for comparison. Note the increased intensity of the triplet emission bands on going from Ar, where none is observed, to Xe, where only triplet emission is observed. The relative intensity of the triplet emission in the Zn–Kr system exhibits a temperature dependence in the range 10–40 K.

co-workers[5] it has been shown by laser pump–probe spectroscopy that the deactivation is entirely due to ISC production of $\mathrm{Zn}(4s4p\ ^3P_{2,1})$.

With regard to equivalent ''half-collision'' studies, which are more comparable to matrix conditions, the $\mathrm{Zn{\cdot}Ar}(^1\Pi_1)$ and $\mathrm{Zn{\cdot}Kr}(^1\Pi_1)$ states fluoresce strongly[6,7] with no evidence for ISC production of $\mathrm{Zn}(4s4p\ ^3P_J)$ states by predissociation. The highest energy $^1\Pi_1(v')$ vibrational states which can be Franck–Condon excited from the ground state are within 150–300 cm^{-1} of the dissociation energies of these $^1\Pi_1$ states. It appears, therefore, that in the Zn·Ar and Zn·Kr cases the repulsive $^3\Sigma_1$ curves do not cross the bound regions of the $^1\Pi_1$ curves. The crossings which do occur for the Zn·Ar and Zn·Kr $^1\Pi_1$ curves are on the inner wall at energies well above the bound regions of spectroscopic interest. In contrast, $\mathrm{Zn{\cdot}Xe}(^1\Pi_1)$ does not fluoresce at all. However, ''action'' spectra, in which a second delayed laser pulse is tuned to a $\mathrm{Zn}(^3P_J)$ atomic transition, allowed characterization of the $\mathrm{Zn{\cdot}Xe}(^1\Pi_1)$ potential curve.[8] The lifetime of the excited $^1\Pi_1$ state of the half-collision Zn·Xe complex has been determined[8] to be 6 ps from linewidth measurements made in the action spectra. The conclusion is that the $\mathrm{Zn{\cdot}Xe}(^3\Sigma_1)$ curve is sufficiently repulsive to cross the deeply bound $\mathrm{Zn{\cdot}Xe}(^1\Pi_1)$ potential curve below the energies of all the $\mathrm{Zn{\cdot}Xe}(^1\Pi_1,v')$ vibrational levels Franck–Condon excited, and probably on the inner wall of the $^1\Pi_1$ curve.[8,9]

As first postulated by Breckenridge and Malmin,[10] collision-induced intersystem crossing of $\mathrm{M}(nsnp\ ^1P_1)$ states to $\mathrm{M}(nsnp\ ^3P_J)$ states is now thought[11] to be caused by spin–orbit-induced, avoided curve crossings of bound $^1\Pi_1$ M·RG state potentials, correlating with $\mathrm{M}(nsnp\ ^1P_1)$ atomic asymptotes, and repulsive $^3\Sigma_1$ M·RG states correlating with $\mathrm{M}(nsnp\ ^3P_2)$. With the availability of triplet $^3\Pi(p_x,p_y)$ state[11] and $^3\Sigma(p_z)$ state[11,12] potentials of the Zn·RG diatomics, the role played by the two lattice vibrations, Q_2 and Q_3, in the corresponding $^1A_1/{}^3E$ predissociative ISC mechanism of matrix-isolated atomic zinc will be examined in this paper. Before the ISC behavior of the Zn–RG matrix systems is examined, that occurring for the $\mathrm{Zn{\cdot}RG}_n$ clusters of relevance to the matrix work will be treated. The $\mathrm{Zn{\cdot}RG}_n$ cluster species in question, with $n=3$, 4, and 5 pertain to triangular, square, and square pyramid arrangements of rare gases, respectively. The objective of the present paper is to see if the pair potential approach, used with success in simulating[1] the matrix luminescence spectroscopy, can also be used to explain the recorded ISC behavior of atomic zinc isolated in the solid rare gases.

TABLE I. Morse $D_e[1-e^{-\beta(R-R_e)}]^2$ and repulsive exponential $Ae^{-\beta(R)}$ functions used as bound and free state pair potentials, respectively, for rare-gas–rare-gas interactions and atomic zinc–rare-gas atom interactions. Data is that quoted in Ref. 11.

Diatomic	D_e (cm^{-1})	R_e (Å)	β ($\mathrm{Å}^{-1}$)	$A(\times 10^{-6}$ $\mathrm{cm}^{-1})$
$\mathrm{Ar–Ar}(X\ ^1\Sigma)$	99.2	3.761	1.685	···
$\mathrm{Kr–Kr}(X\ ^1\Sigma)$	138.4	4.017	1.604	···
$\mathrm{Xe–Xe}(X\ ^1\Sigma)$	196.24	4.3634	1.509	···
$\mathrm{ZnAr}(X\ ^1\Sigma)$	95	4.18	1.001	···
$\mathrm{ZnKr}(X\ ^1\Sigma)$	115	4.2	0.922	···
$\mathrm{ZnXe}(X\ ^1\Sigma)$	162	4.4	0.828	···
$\mathrm{ZnAr}(^1\Pi)$	700	2.97	1.429	···
$\mathrm{ZnKr}(^1\Pi)$	1400	2.80	1.594	···
$\mathrm{ZnXe}(^1\Pi)$	3241	2.83	1.649	···
$\mathrm{ZnAr}(^3\Pi)$	487	3.23	1.378	···
$\mathrm{ZnKr}(^3\Pi)$	800	3.1	1.692	···
$\mathrm{ZnXe}(^3\Pi)$	1400	3.0	1.75	···
$\mathrm{ZnAr}(^1\Sigma)$	···	···	1.615	0.50
$\mathrm{ZnKr}(^1\Sigma)$	···	···	1.600	0.55
$\mathrm{ZnXe}(^1\Sigma)$	···	···	1.725	1.00
$\mathrm{ZnAr}(^3\Sigma)$	···	···	1.588	0.54
$\mathrm{ZnKr}(^3\Sigma)$	···	···	1.558	0.598
$\mathrm{ZnXe}(^3\Sigma)$	···	···	1.700	1.079

II. METHODS

A. Theoretical simulations

The theoretical methods used in the cluster[11] and matrix[1] calculations have already been published so presentation here will be restricted to detail pertaining specifically to the ISC mechanism. The molecular constants of the bound excited $^{1,3}\Pi$ $\mathrm{Zn}(p_x,p_y)\cdot\mathrm{RG}$ state potentials, $V_{1,3_\Pi}(R)$, have been estimated from experimental data[11] and are described by Morse functions. The repulsive excited $^{1,3}\Sigma$ $\mathrm{Zn}(p_z)\cdot\mathrm{RG}$ state potentials, $V_{1,3_\Sigma}(R)$, are described by repulsive exponential functions, obtained by fitting[11] analytic functions of the form $V(R)=Ae^{-\beta(R)}$ to the calculated *ab initio* points.[12] The parameters of these molecular potentials are collected in Table I.

The cluster calculations were all performed with the rare-gas–rare-gas distances set at the bond lengths of the rare gas dimer molecules whose values are collected in Table II. The matrix calculations were performed for a quasi-molecular $\mathrm{Zn–RG}_{18}$ cluster species composed of the 12

TABLE II. The rare-gas–rare-gas distances used in the $Zn\cdot RG_n$ clusters are the bond lengths, r_e, of the ground electronic state listed in Table I for the rare-gas dimer molecules. The distance, *r*, is the distance each rare-gas atom is from the center of mass of the planar rare-gas clusters or, in the RG_5 case, to the base of the square pyramid structure. The value *r* is obtained using the formulae $r=r_e/\sqrt{3}$, $r_e/\sqrt{2}$, and $r_e/\sqrt{2}$ which pertain to the triangular, square, and square pyramid structures of the $Zn\cdot RG_3$, $Zn\cdot RG_4$, and $Zn\cdot RG_5$ cluster species, respectively. All distances are in Angstrom units.

RG	$r_e(RG_2)$	$r(RG_3)$	$r(RG_4)$	$r(RG_5)$
Ar	3.761	2.171	2.659	2.659
Kr	4.017	2.319	2.840	2.840
Xe	4.363	2.519	3.085	3.085

nearest-neighbor rare-gas atoms in the first sphere surrounding the zinc atom in the substitutional site, at a distance $R=a/\sqrt{2}$, and the six atoms in the second surrounding sphere, at a distance of the lattice parameter $R=a$ from the zinc atom. The lattice parameters, *a*, and site diameters for the solid rare gases are collected in Table III.

The key expressions[1,11,13] for ISC in the cluster and matrix systems are the following functions:

$$W_{1_{A1}}(R)=\sum_{j=1}^{n}[\cos^2\theta_j V_{1_\Sigma}(R_j)+\sin^2\theta_j V_{1_\Pi}(R_j)], \quad (1)$$

$$W_{3_E}(R)=\sum_{j=1}^{n}[\sin^2\theta_j V_{3_\Sigma}(R_j)+(\cos^2\theta_j+1)V_{3_\Pi}(R_j)], \quad (2)$$

which give the energy of the strongly bound $^1A_1$ state and the repulsive ^3E states for *n* Zn–RG pairs of interactions considered. In these expressions $V_{1_\Pi}(R)$ and $V_{1_\Sigma}(R)$ are the bound and repulsive excited singlet *p*-state potentials, respectively, of the diatomic Zn·RG molecules, while $V_{3_\Pi}(R)$ and $V_{3_\Sigma}(R)$ are the spin triplet equivalents. θ_j is the angle between the axis of atomic zinc motion, the ''approach axis,'' and the position of a particular rare-gas atom in a cluster or in an fcc lattice.

The summation in the general expressions given by Eqs. (1) and (2) for a $Zn\cdot RG_n$ cluster can be replaced by more manageable products when calculating the energies of high symmetry C_{nv} species. Thus for the $Zn\cdot RG_3$ and $Zn\cdot RG_4$ clusters the expressions for the $^1A_1$ and ^3E states are

TABLE III. Site sizes (Å units) in the solid rare gases calculated from the lattice parameters, *a*, of the unit cells (Ref. 21) at 4 K. The diameter of a substitutional site in a face centered cubic solid is $ss=a/\sqrt{2}$, while the octahedral interstitial site diameter, I_{Oh} (located at the center of the fcc unit cell) is the lattice parameter minus the substitutional site diameter, $a-ss$. The internal diameter of the tetrahedral interstitial site I_{Td} is $(\sqrt{3}/\sqrt{2}-1)\times ss$. The *radius* of the tetra-vacancy site (removal of four rare gas atoms surrounding the I_{Td} site) is the substitutional site *diameter* *ss*, plus the *radius* of the tetrahedral interstitial site.

	a	*ss*	I_{Td}	I_{Oh}	Tet.vacan
Ar	5.312	3.756	0.844	1.556	8.356
Kr	5.644	3.991	0.897	1.653	8.879
Xe	6.131	4.335	0.974	1.796	9.644

$$W_{1_{A1}}(R)=n[\cos^2\theta V_{1_\Sigma}(R)+\sin^2\theta V_{1_\Pi}(R)], \quad (3)$$

$$W_{3_E}(R)=\frac{n}{2}[\sin^2\theta V_{3_\Sigma}(R)+(\cos^2\theta+1)V_{3_\Pi}(R)], \quad (4)$$

where $n=3$ and 4. For the square pyramidal, C_{4v} $Zn\cdot RG_5$ species, the term $V_{1_\Sigma}(R+r)$ must be added on to Eq. (3) and the term $V_{3_\Pi}(R+r)$ added to Eq. (4), with $n=4$ in both equations, to obtain the energies of the bound $^1A_1$ and repulsive ^3E states, respectively. In the $Zn\cdot RG_5$ systems, *r* is the distance of the rare-gas atom on the apex of the square pyramid to the base of the square pyramid, which is a constant, given the rigid cluster calculations done. As outlined in the preceding[14] and earlier articles,[1] the fourfold symmetry of the fcc rare-gas lattices allows the 18 rare-gas atoms considered in the $Zn\cdot RG_{18}$ matrix calculations to be categorized into four groups. Expressions similar to those listed above for the square planar $Zn\cdot RG_4$ and square pyramid $Zn\cdot RG_5$ cluster species listed above are used for the atoms in these categories. Further details are to be found in the preceding[14] and earlier publications.[1]

III. RESULTS AND DISCUSSION

A. Rare-gas clusters

The approach taken in the analysis of ISC is an extension of the proposal made originally by Breckenridge and Malmin[10] in their gas-phase study of the quenching of excited *p*-state metal atoms by rare-gas atoms. In particular it was proposed that the efficiency of $^1P_1-^3P_J$ intersystem crossing in these systems was related to whether a predissociative curve crossing occurs between a strongly bound $^1\Pi_1$ state and a repulsive $^3\Sigma_1$ state for the M·RG diatomics. This mechanism has recently been extended by the Salt Lake City group[11] in an analysis of the ISC in $M\cdot RG_n$ (M=Mg and Zn) cluster species for $n=2$ and 3. The bound $^1A_1$ and repulsive ^3E state potentials responsible in this kind of predissociative ISC mechanism for the $M\cdot RG_n$ cluster species ($n=3$, 4, and 5) and the Zn/RG matrix systems of interest here are given explicitly by Eqs. (1) and (2), respectively, for the *n* M·RG interactions in the cluster.

Predictions of ISC in the $Zn\cdot RG_n$ cluster species were made by examining whether curve crossing of the bound $^1A_1$ and repulsive ^3E states occurred for the perpendicular approach of the excited *p*-state Zn atom to the rare-gas clusters. The rare-gas–rare-gas bond lengths in these potential-energy calculations are all set at those of the rare-gas dimers, listed in column two of Table II, while the geometries of the $Zn\cdot RG_3$, $Zn\cdot RG_4$, and $Zn\cdot RG_5$ clusters are fixed as triangular, square, and square pyramid, respectively. The sizes of the planar RG_3 and RG_4 cluster species are indicated in Table II by the distance, *r*, of each rare-gas atom to the center of the cluster. For the square pyramidal RG_5 cluster *r* is the distance of each rare-gas atom to the center of the base of the square pyramid.

Results of the present $Zn\cdot RG_3$ calculations are shown in Fig. 2. In agreement with the earlier work of Kaup and Breckenridge,[11] a $^1A_1/^3E$ crossing does not occur for $Zn\cdot Ar_3$. A crossing is found in the Kr system but, as shown

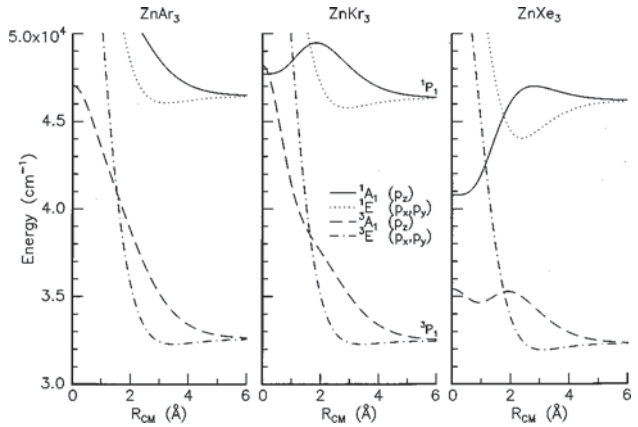

FIG. 2. Potential-energy diagrams for the excited electronic singlet and triplet states in the $Zn\cdot RG_3$ complexes. The diagrams show the variation in energy for the perpendicular approach of the zinc atom to the center of an equilateral triangle arrangement of the three rare-gas atoms. The variable, R_{CM}, is the distance of the zinc atom to the center-of-mass of the planar RG_3 species, where $R_{CM}=0$. In the resulting threefold C_{3v} symmetry, the p_x and p_y orbital orientations are equivalent and degenerate with E designation, while the p_z orientation is A_1. Both of these orbital states have spin singlet and triplet versions whose asymptotic limits are determined by the atomic zinc singlet $4p\ ^1P_1$ and triplet $4p\ ^3P_1$ energy levels, respectively. Note that only in the $Zn\cdot Xe_3$ system does the bound $^1A_1$ state (solid curve) cross the repulsive ^3E state (dot–dash curve) at an energy lower than the atomic zinc $4p\ ^1P_1$ asymptote.

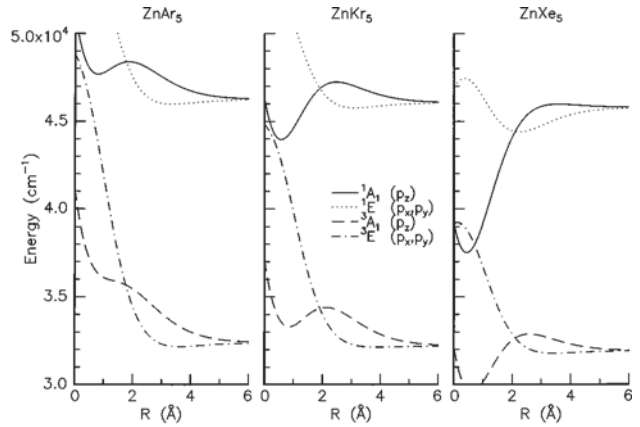

FIG. 4. Perpendicular approach of a p-state Zn atom, along the symmetry axis, to the base of a square pyramid of five rare-gas atoms. The variable R is the distance to the base of the square pyramid. The influence of the apical rare-gas atom can be seen by comparing with the curves obtained for $Zn\cdot RG_4$ cluster species. Particularly noteworthy is the decrease in the binding energy of the A_1 states due to the repulsive p_z σ-type interaction between the approaching zinc and the rare-gas atom on the apex of the pyramid. A reduction in the repulsion of the E states also arises because of the attractive p_x and p_y π-type interaction which this atom has with the approaching zinc. In this case only the $Zn\cdot Xe_5$ cluster shows a $^1A_1/^3E$ curve crossing.

in the middle panel in Fig. 2, at an energy in excess of the $^1P_1$ asymptote. Only in the $Zn\cdot Xe_3$ cluster is there a $^1A_1/^3E$ crossing which will promote ISC. In contrast to the $Zn\cdot RG_3$ species we find, as shown in Fig. 3, that all the $Zn\cdot RG_4$ species exhibit $^1A_1/^3E$ curve crossings. The situation for the approach of a $^1P_1$ Zn atom to a square pyramid of five rare-gas atoms, shown in Fig. 4, is quite different to the $Zn(^1P_1)\cdot RG_4$ species in that only the $Zn\cdot Xe_5$ cluster shows curve crossing. While the rigid C_{4v} $Zn\cdot RG_5$ cluster species may be of little significance in the gas phase, they are of particular importance in the solid environment of rare-gas matrices since they represent the octahedral interstitial sites into which the excited p-state Zn atoms can migrate from an originally occupied substitutional site.

A summary of the ISC predictions for the $Zn\cdot RG_n$ clusters, based on $^1A_1/^3E$ curve crossings, is presented in Table IV. These results show that ISC is: a) much more favorable for the xenon clusters than the argon and krypton clusters and b) depends strongly on the geometry of the Ar and Kr clusters. As noted by Kaup and Breckenridge[11] the Franck–Condon factors for excitation of the ground-state $Zn\cdot RG_3$ clusters are such that the outer repulsive regions of the $^1A_1$ states are accessed where a barrier intervenes in reaching the strongly attractive region. It is the much less strongly bound ^1E states which will be accessed in optical absorption. Thus,

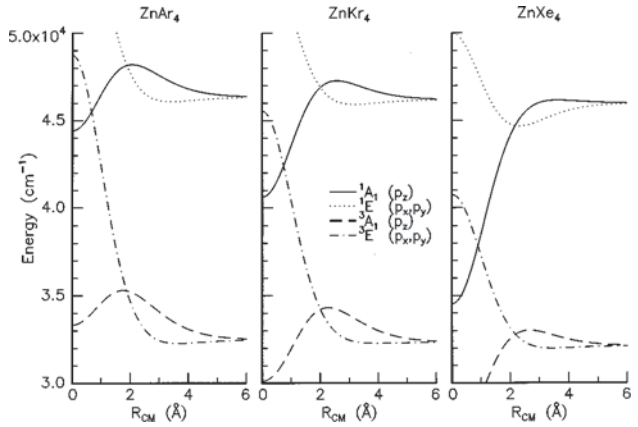

FIG. 3. Energetics for the perpendicular approach of the excited p-state zinc atom to four rare-gas atoms arranged as a square. All other parameters as in Fig. 2. Note, in contrast to the $Zn\cdot RG_3$ curves, how curve crossing between the bound $^1A_1$ (solid curve) and the repulsive ^3E (dot–dash curve) occur at energies lower than the atomic $^1P_1$ asymptote for all the $Zn\cdot RG_4$ cluster species.

TABLE IV. Predictions for ISC in $Zn\cdot RG_n$ rigid model clusters and Zn–RG matrix systems based on the crossing or noncrossing of the bound spin singlet $^1A_1$ and repulsive spin triplet ^3E states. The entries indicated by ''yes'' pertain to situations where a $^1A_1/^3E$ curve crossing occurs at an energy lower than that reached in a Franck–Condon absorption transition. The calculations for the $Zn\cdot RG_3$ and $Zn\cdot RG_4$ species correspond to the perpendicular approach of a p-state Zn atom to the center of a triangular and square arrangement of the rare-gas atoms. That of the $Zn\cdot RG_5$ is for a similar approach to the base of a square pyramid of rare-gas atoms. During the calculations all of the rare-gas bond lengths are held fixed at the values of the ground-state dimers. The matrix calculations shown in the two columns under the revised heading were performed with the ''recommended'' $^3\Sigma(p_z)$ state potentials quoted in Ref. 11 and listed in Table V. All others used the repulsive $^3\Sigma(p_z)$ state potentials obtained from *ab initio* calculations and listed in Table I.

	$Zn\cdot RG_3$	$Zn\cdot RG_4$	$Zn\cdot RG_5$	Zn–RG Q_2	Zn–RG Q_3	Revised Q_2	Revised Q_3
Ar	no	yes	no	yes	yes	no	no
Kr	no	yes	no	yes	yes	no	yes
Xe	yes	yes	yes	yes	yes	yes	yes

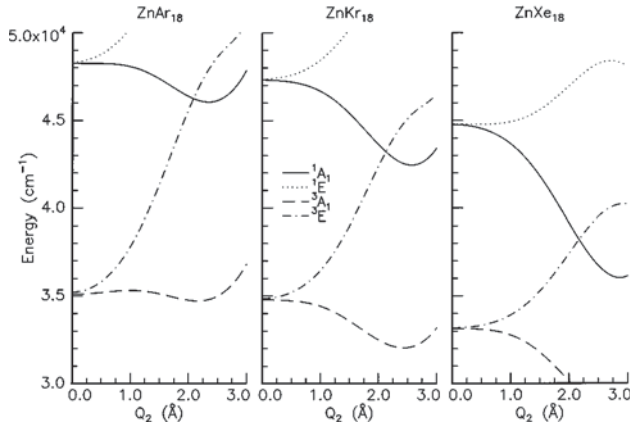

FIG. 5. Energies of the spin singlet and triplet A and E states of the Zn–RG matrix systems as predicted for a $Zn{\cdot}RG_{18}$ cluster. The vibrational mode shown is the body mode Q_2 which corresponds to the motion of the zinc atom out of the substitutional site occupied by the zinc atom in the ground $^1S_0$ state ($R=0$) and towards an adjacent octahedral interstitial site. Note how curve crossings between the bound $^1A_1$ (solid curve) and the repulsive ^3E (dot–dash curve) curves occur for all the Zn–RG systems.

while the deeply bound $^1A_1$ state crosses the ^3E state in several of these clusters, the presence of a barrier between the region of the $^1A_1$ potential accessed in absorption, precludes reaching the $^1A_1/^3E$ crossing point. It is only in the $Zn{\cdot}Xe_4$ species, where a crossing at the minimum of the bound ^1E state by the $^1A_1$ state occurs, that ISC may experimentally be observed following laser excitation from the ground state.

B. Rare-gas solids

In a simulation of the ISC occurring in the solid-state environment of the matrix, 18 distance and angle terms are taken into account to generate the $^1A_1$ and ^3E curves using Eqs. (1) and (2), respectively. The results of these calculations are shown in Figs. 5 and 6 as a function of the two

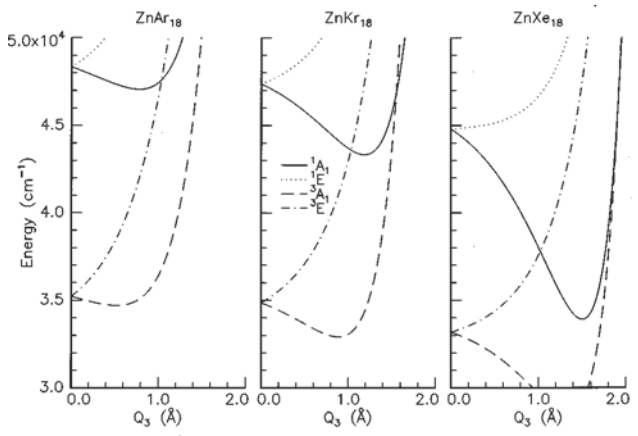

FIG. 6. Energies of the spin singlet and triplet A and E states of the Zn–RG matrix systems as a function of the waist mode, Q_3. This motion corresponds to the in-phase contraction of four nearest-neighbor rare-gas atoms towards the zinc atom. $R=0$ pertains to the undistorted substitutional site occupied by the zinc atom in the ground $^1S_0$ state. As with the body mode calculations, note how $^1A_1/^3E$ curve crossings occur for this mode in all the Zn–RG systems.

vibronic modes considered, the body and waist modes Q_2 and Q_3. It can be seen in these figures that $^1A_1/^3E$ curve crossings occur in all the Zn–RG matrix systems. ISC predictions based on these crossings are presented in the center columns in Table IV, in which it appears that the two modes induce ISC in all of the Zn–RG systems.

The ISC predictions for the Zn–Ar system, based on $^1A_1/^3E$ curve crossings, are clearly at variance with the recorded luminescence, shown in Fig. 1, in that no triplet emission is observed in the temperature range accessible in solid argon, i.e., $T<33$ K and only a minor amount of triplet is present in Kr. To ascertain the reason for this disagreement, the assumptions implicit in the calculations were reexamined. Since the ISC behavior in the Zn–Ar system is particularly clear-cut, the reason for the large discrepancy in the theoretical predictions was sought in detail for this system.

Two factors are considered in this regard. The first, particular to the Zn–Ar system, relates to the site occupancy that atomic zinc will have in the solid Ar host. The other, which is generally applicable to the Zn–RG systems, is the reliability of the repulsive $^3\Sigma_1$ potential curves taken directly from the *ab initio* calculations[12] and used to represent the repulsive triplet $^3\Sigma(p_z)$ curves of the $Zn{\cdot}RG$ diatomics.

C. Site occupancy in Zn–Ar

Because of the mismatch in the equilibrium internuclear separation of $Zn{\cdot}Ar$ in the ground electronic state, 4.18 Å, and that of Ar dimer, 3.76 Å, it is expected that occupancy of atomic zinc in a substitutional site of an undisturbed Ar lattice will be cramped. The method used to determine the dimensions of the site of isolation of atomic Zn in a relaxed Ar lattice has been presented in the preceding article[14] and elsewhere,[15] indicating a site 0.122 Å larger than the diameter of a substitutional site of an undistorted Ar lattice.

When the $^1A_1$ and ^3E curves of the body and waist modes were recalculated with this 0.122 Å increase in the substitutional site diameter, curve crossing still occurred for both modes.[15] Thus we conclude that the size of the Ar site accommodating the guest Zn atom has only a minor effect on the ISC process. The lattice relaxation procedure outlined for the Zn–Ar system was repeated[15] for the Zn–Kr and Zn–Xe systems indicating substitutional site expansion of only 0.057 and 0.002 Å for Kr and Xe, respectively. These values are so small that $^1A_1/^3E$ curve crossings are not changed from the results obtained for the undisturbed Kr and Xe lattices.

D. Refining the $^3\Sigma$ state potential

The factor which plays the most important role in the ISC, and a possibility which must be considered, is the accuracy of the repulsive exponential functions in Table I used to represent the repulsive triplet $^3\Sigma_1(p_z)$ curves of the $Zn{\cdot}RG$ diatomics. As mentioned in the Introduction, these curves have been determined by fitting analytic functions to the calculated *ab initio* points, but as pointed out by Kaup and Breckenridge,[11] the *ab initio* points are expected to be somewhat higher in energy than the true values. In their

TABLE V. Repulsive exponential $Ae^{-\beta(R)}$ functions used to represent the free ($^3\Sigma$) state pair potentials of the atomic zinc–rare-gas atom interactions. The β coefficient has units (Å^{-1}), the A term (cm^{-1}). Data is that quoted in Ref. 11.

	Ab initio		Intermediate		Recommended	
Diatomic	A	β	A	β	A	β
ZnAr	540 000	1.588	500 000	1.615	450 000	1.640
ZnKr	598 000	1.558	550 000	1.600	500 000	1.625
ZnXe	1 079 000	1.700	1 000 000	1.725	950 000	1.750

paper,[11] more reasonable values for the repulsive exponential functions are given to describe the $^3\Sigma_1(p_z)$ states of the Zn·RG diatomics. These less repulsive potentials, chosen consistently, were in good agreement with the experimental observations made on the Zn·RG diatomic molecules: A $^1\Pi_1/^3\Sigma_1$ crossing for Zn·Xe, where efficient ISC occurs[8] by $^1\Pi_1$ predissociation; and no energetically accessible $^1\Pi_1/^3\Sigma_1$ crossings for Zn·Ar and Zn·Kr, which do not exhibit[6,7] ISC. The values of these less repulsive $^3\Sigma_1$ potentials are collected in Table V for Zn·Ar, Zn·Kr, and Zn·Xe.

Using the recommended values for the $^3\Sigma_1(p_z)$ states quoted in Ref. 11 and listed in Table V, the matrix-ISC calculations were repeated, the results of which are presented in Figs. 7 and 8 for the body and waist modes, respectively. As shown in Fig. 7, $^1A_1/^3E$ curve crossing does not occur now for the body mode, Q_2, of the Zn–Ar system. The crossing which occurs on the waist mode, Q_3, is, as shown in Fig. 8, at an energy 1694 cm^{-1} above that accessed in absorption ($R=0$). Thus a $^1A_1/^3E$ curve crossing which will promote ISC after photoexcitation in the Zn–Ar matrix system does not occur. The situation in the Zn–Xe system is clear-cut, showing $^1A_1/^3E$ curve crossings for both modes in agreement with luminescence observations. A summary of the revised ISC predictions obtained with the less repulsive $^3\Sigma$ curve is shown in the two columns on the extreme right in Table IV.

The situation for the Zn–Kr system is more complex in that the body mode does not show a crossing, Fig. 7, while the waist mode, Fig. 8, shows a crossing of the repulsive ^3E curve close to the energy minimum of the bound ^1A curve. It will be remembered that the weak 238 nm emission in the Zn–Kr system was assigned in Ref. 1 to the waist mode while the more intense 258 nm band was assigned to the body mode. Could it be that the difference in intensity of the two singlet bands in the Zn–Kr system is due, as predicted in the pair potentials calculations, to ISC promoted by the waist mode but not on the body mode? A problem which arises in this regard, however, is why the ISC in the Zn–Xe system is so much more efficient than that occurring for the same mode in the Zn–Kr system. To examine this difficulty in more detail, the singlet to triplet hopping probabilities are calculated in both systems.

E. Landau–Zener surface hoppings

Estimates of the $^1A_1/^3E$ surface hopping efficiencies are obtained from Landau–Zener (LZ) theory. The potential curves we calculate are diabats and in LZ theory the probability of staying on the original singlet [$V_{^1A_1}(R)$, curve 1] diabat is obtained using the formula[16]

$$P_{\text{LZ}}=\exp\left(-\frac{4\pi^2V_{12}^2}{h\nu|F_1-F_2|}\right), \tag{5}$$

in which ν is the nuclear velocity of the particles at the crossing point, r_c, while F_1 and F_2 are the gradients of the spin singlet and triplet diabats at this point. For diatomic systems, the hopping probability between the two diabatic curves is $P_{12}=2P_{\text{LZ}}(1-P_{\text{LZ}})$ since two traversals of the crossing point occur. For a single pass through the crossing point, as is likely to be the case in a rapidly relaxing solid-state system, the hopping probability from the singlet [$V_{^1A_1}(R)$, curve 1] to the triplet state potential [$V_{^3E}(R)$, curve 2] is $1-P_{\text{LZ}}$.

The matrix element, V_{12}^2, coupling the two potentials is derived from the spin-orbit coupling term whose magnitude depends firstly, on the metal atom considered and secondly, on the spatial symmetries of the interacting states. The spin-orbit coupling constant, ζ, of the $4s4p$ configuration of atomic zinc is $\zeta_{4p}=2(E_{^3P_2}-E_{^3P_0})/3$ which from Moore's Tables has a value of 386.0 cm^{-1}. The coupling term for the $^1\Pi_1/^3\Sigma_1$ states of the Zn·RG diatomics[12,17,18] is one half the spin-orbit coupling constant of the free atom, $V_{12}=\zeta/2$. For the $^1B_1/^3A_1$ states[18] of the Zn·RG$_2$ clusters in C_{2v} symmetry, $V_{12}=\sqrt{2}\zeta/4$ and for the $^1A_1/^3E$ states in the C_{nv} symmetry Zn·RG$_n$ clusters, where $n\geqslant 3$, $V_{12}=\zeta/\sqrt{2}$.

As for diatomic molecules, the nuclear velocity, ν, at the crossing point can be obtained from the expression $\nu=\sqrt{(2E_{\text{Kin}}/\mu)}$ in which μ is the reduced mass and E_{Kin} is the kinetic-energy obtained from the energy difference between the region of the singlet $^1A_1$ potential accessed in Franck–Condon absorption and the crossing point, r_c. A question arises, however, in the case of a rapidly relaxing solid-state system, as to whether this is the correct choice of the nuclear

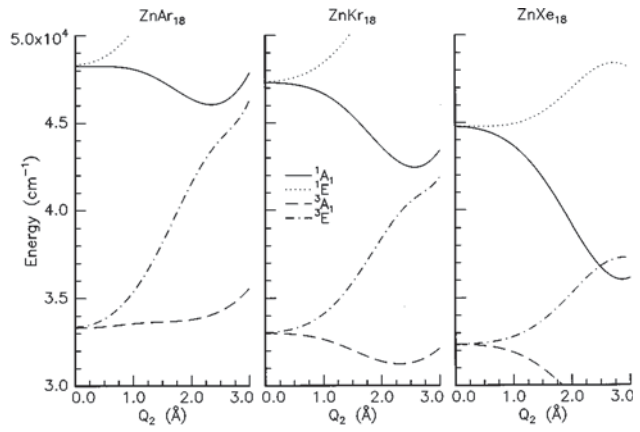

FIG. 7. Identical body mode calculations for the Zn–RG matrix systems as those shown in Fig. 5, except that the repulsive exponential function for the $^3\Sigma$ state is less repulsive than the *ab initio* points used in the earlier plot (see Table V ''recommended'' potentials). Note how a $^1A_1/^3E$ curve crossing occurs now in the Zn–Xe system only. The lack of such a crossing in the Zn–Ar and Zn–Kr systems is consistent with the observation of strong singlet emissions at 238 and 258 nm in these two systems, respectively, both of which have been assigned in Ref. 1 to the body mode.

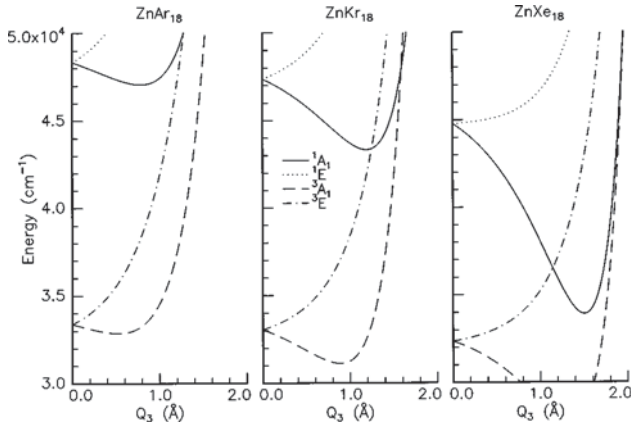

FIG. 8. Repeat of the waist mode calculations shown in Fig. 6 but with the less repulsive $^3\Sigma$ state potentials used in Fig. 7. Note how the $^1A_1/^3E$ curve crossing in the Zn–Ar system occurs at an energy in excess of that reached in absorption. $^1A_1/^3E$ curve crossing does occur in the Zn–Kr and Zn–Xe systems, in line with the presence of a very weak singlet waist mode emission at 238 nm in Kr and its complete absence in Xe.

velocity term. It seems unlikely that the total amount of kinetic energy will be available at the crossing point of the solid-state system as is the case for a gas-phase molecule. Considering that the relaxation in the solid-state systems is facilitated by rapid energy transfer to phonon modes of the lattice, a more likely possibility is that the maximum kinetic energy available at the crossing point is the highest phonon frequency in the solid host, resulting in a much reduced nuclear velocity term ν' and a lower limit to the hopping probability. Estimates of the LZ hopping probabilities are obtained for both molecular and ''phonon'' velocities and the values are quoted in Table VI. Furthermore, instead of the reduced mass which appears in the velocity expression for diatomics, only the masses of the atoms undergoing motion in a particular vibrational mode are considered in the solid. In the waist mode Q_3 of the excited $^1A_1$ electronic state of the $Zn{\cdot}RG_{18}$ cluster used to represent the solid matrix, it is only the four nearest rare-gas neighbor atoms which are undergoing an in-phase vibrational motion. Similar to the a_{1g} vibrational mode of a square planar XY_4, D_{4h} polyatomic[19] molecule, for which only the mass of one end Y atom is used to obtain the vibrational frequency, the effective reduced mass, μ', for the waist mode in the solid-state Zn–Kr or Zn–Xe systems is simply the atomic mass of Kr or Xe.

TABLE VI. Parameters used in Landau–Zener calculations of the probability of $^1A_1$ to ^3E state hoppings at the curve crossing found for the waist modes Q_3 in the Zn–Kr and Zn–Xe systems. ΔF is the absolute value of the difference of the slopes, F_1 and F_2 whose values at the crossing points are shown in the panels on the right of Fig. 9. K is the product of V_{12}^2 and the physical constants appearing in Eq. (5), while ν and ν' are the nuclear velocities calculated for molecular and solid-state systems, respectively; see text. Two sets of probabilities are shown for the two possible selections of the nuclear velocities. The underlined values are relevant to ISC in the solid state.

	Zn–Kr	Zn–Xe
ΔF (cm^{-1}/Å)	25384.6	21222.1
K($m\,s^{-1}$)	347.3	415.5
ν ($m\,s^{-1}$)	1091.1	1229.8
P_{LZ}	0.727	0.713
$\underline{(1-P_{LZ})}$	$\underline{0.273}$	$\underline{0.287}$
P_{12}	0.397	0.409
ν' ($m\,s^{-1}$)	134.0	95.9
P'_{LZ}	0.075	0.013
$\underline{(1-P'_{LZ})}$	$\underline{0.925}$	$\underline{0.987}$
P'_{12}	0.138	0.026

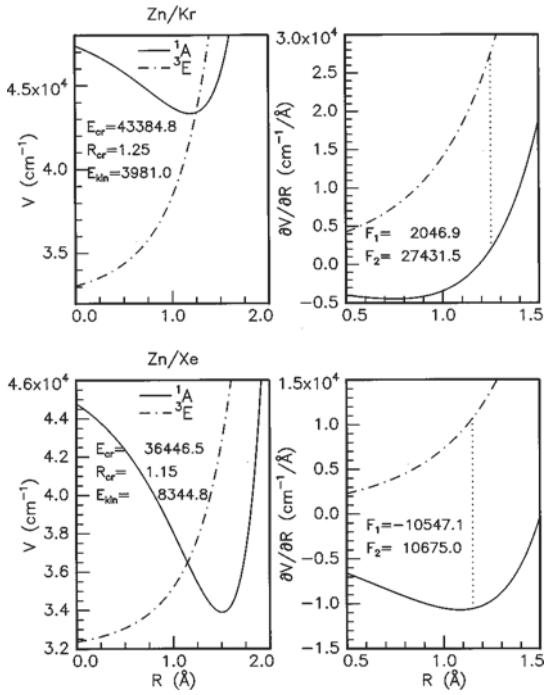

FIG. 9. Details of the $^1A_1$ to ^3E state curve crossings occurring on the waist modes, Q_3, in the Zn–Kr and Zn–Xe matrix systems and numerical values used in Landau–Zener calculation for the hopping probabilities. The panels on the left show the potential-energy curves of the $^1A_1$ to ^3E states as well as numerical details of the crossing points. The panels on the right show the gradients calculated in the vicinities of these crossing points. The dotted vertical lines in the panels on the right hand side indicate the locations of the crossing points used to determine the values of F_1 and F_2 in Eq. (5). E_{Kin} is the kinetic-energy calculated as the difference between the region of the $^1A_1$ state reached in a Franck–Condon absorption from the ground state ($R = 0$ Å in the potential plots) and the energy at the crossing point E_{CR}.

Details of the $^1A_1$ and ^3E state crossing points found for the waist mode Q_3 in the Zn–Kr and Zn–Xe systems are presented in Fig. 9 as well as the numerical values extracted for use in the LZ calculations. The LZ results on the waist mode $^1A_1/^3E$ state interactions in the Zn–Kr and Zn–Xe matrix systems indicate, as listed in Table VI, equal but small hopping probabilities for both systems, $1-P_{LZ} = 0.273$ and 0.287, respectively, assuming the full Franck–Condon kinetic energy is available. The value for the Zn–Xe system is clearly much smaller than what is required for complete quenching of the singlet emission. In light of this underestimation of the $^1A_1/^3E$ hopping probability, the parameter most suspect in the LZ calculation is the use of the nuclear velocity obtained as the full energy difference between the Franck–Condon region accessed in absorption and the crossing point. If, as mentioned above a reduced nuclear velocity term, ν', pertaining to maximum phonon[20] frequencies of 60 and 50 cm^{-1} are used for Kr and Xe, respectively,

then $1-P'_{LZ}$ values of 0.925 and 0.987 are found which are much more consistent with observations in the Zn–Xe system.

The very large differences in ISC exhibited in the Zn–Kr and Zn–Xe systems is then clearly not arising because of the hopping probabilities which are calculated to be large in both systems. A closer examination of the crossing in the waist mode of the Zn–Kr system, top left panel of Fig. 9, reveals that the $^1A_1/^3E$ curves cross 0.06 Å beyond the energy minimum of the bound $^1A_1$ state and 60.2 cm^{-1} above it. If, as is usually expected in solid-state luminescence, thermal relaxation due to interactions with the phonon bath is very fast, then it may be that the $^1A_1/^3E$ crossing in the Zn–Kr system is, for dynamics reasons, not reached or reached infrequently at low temperatures. Indeed a kinetics measurement[2] of the temperature dependence exhibited in the triplet emission in the Zn–Kr system revealed a barrier height of 38.6 cm^{-1} for ISC. When zero-point energy of 20 cm^{-1} at the minimum of the waist mode of the $Zn\cdot Kr_{18}$ complex is taken into account, the close agreement between the observed activation energy barrier and the crossing point (40 cm^{-1}) is impressive but perhaps fortuitous?

Since, in the activated ISC process of Zn–Kr the crossing point is reached by thermal population of the low-energy phonon levels, then use of the standard LZ hopping probability, $P'_{12}=2P'_{LZ}(1-P'_{LZ})$ would seem appropriate, under these specific conditions. In this case the hopping probability found is 0.14, see Table VI, a value still consistent with efficient thermal quenching of the singlet fluorescence. In the Zn–Xe system, the $^1A_1/^3E$ crossing occurs before the energy minimum of the bound $^1A_1$ state is reached. Thus, all the excited singlet state population relaxing after optical excitation will pass once through this crossing point, where the hopping probability is large, $1-P'_{LZ}>0.99$, and proceed along the ^3E surface to decay eventually as long lived triplet-to-singlet emission.

IV. CONCLUSIONS

Predictions of Zn–RG matrix intersystem crossing based on $^1A_1/^3E$ curve crossings calculated using recommended $^3\Sigma(p_z)$ Zn·RG state potentials are in good agreement with the luminescence observations. In the Zn–Ar system, where only singlet emission is observed, $^1A_1/^3E$ curve crossings do not occur for either body or waist modes. In the Zn–Xe system ISC is so efficient that only triplet emission is observed, and theory predicts that both modes show $^1A_1/^3E$ curve crossings. Indeed the theory appears not only to be able to explain the differences in the efficiency of ISC between the rare gases but also in the Zn–Kr system, between the two vibronic modes which determine the luminescence. The body mode in this system does not exhibit a crossing with the repulsive ^3E state and emits strongly at 258 nm, while the waist mode is crossed and emits weakly at 238 nm.

[1] J. G. McCaffrey and P. N. Kerins, J. Chem. Phys. **106**, 7885 (1997).
[2] V. A. Bracken, P. N. Kerins, P. Gürtler, and J. G. McCaffrey, J. Chem. Phys. **107**, 5300 (1997).
[3] V. A. Bracken, P. Gürtler, and J. G. McCaffrey, J. Chem. Phys. **107**, 5290 (1997).
[4] M. Czajkowski, E. Walentynowics, and L. Krause, J. Quant. Spectrosc. Radiat. Transf. **28**, 493 (1982).
[5] H. Umemoto, T. Ohnuma, H. Ikeda, S. Tsunashima, K. Kuwahara, F. Misaizu, and K. Fuke, J. Chem. Phys. **97**, 3282 (1992).
[6] I. Wallace, R. R. Bennett, and W. H. Breckenridge, Chem. Phys. Lett. **153**, 127 (1988).
[7] I. Wallace, J. Ryter, and W. H. Breckenridge, J. Chem. Phys. **96**, 136 (1992).
[8] I. Wallace, J. G. Kaup, and W. H. Breckenridge, J. Phys. Chem. **95**, 8060 (1991).
[9] S. Bililign, J. G. Kaup, and W. H. Breckenridge, J. Phys. Chem. **99**, 7878 (1995).
[10] W. H. Breckenridge and O. K. Malmin, J. Chem. Phys. **74**, 3307 (1981).
[11] J. G. Kaup and W. H. Breckenridge, J. Phys. Chem. **99**, 13701 (1995).
[12] S. Bililign, M. Gutowski, J. Simons, and W. H. Breckenridge, J. Chem. Phys. **99**, 3815 (1993).
[13] J. Zuniga, A. Bastida, A. Requena, N. Halberstadt, and J. Beswick, J. Chem. Phys. **98**, 1007 (1993).
[14] P. N. Kerins and J. G. McCaffrey, J. Chem. Phys. **109**, 3131 (1998), preceding paper.
[15] P. N. Kerins, Masters Thesis, National Univ. of Ireland, Maynooth, 1998
[16] H. Eyring, J. Walter, and G. E. Kimball, *Quantum Chemistry* (Wiley, New York, 1944), pp. 326–329.
[17] H. Lefebvre-Brion and R. W. Field, *Perturbations in the Spectra of Diatomic Molecules* (Academic, New York, 1986), Chap. 6.
[18] S. Bililign, M. D. Morse, and W. H. Breckenridge, J. Chem. Phys. **98**, 2115 (1993).
[19] G. Herzberg, *Molecular Spectra and Molecular Structure, Vol. II, Infrared and Raman Spectra of Polyatomic Molecules* (Krieger, Florida, 1991), Chap. 4.
[20] N. Schwentner, E. E. Koch, and J. Jortner, *Electronic Excitation in Condensed Rare Gases* (Springer-Verlag, New York, 1985), Chap. 6.
[21] G. L. Pollack, Rev. Mod. Phys. **36**, 748 (1964).